Applied Physics Letters ARTICLE scitation.org/journal/apl

A tunable electromagnetic acoustic switch

Cite as: Appl. Phys. Lett. **116**, 183502 (2020); doi: 10.1063/5.0008532
Submitted: 28 March 2020 · Accepted: 8 April 2020 ·
Published Online: 4 May 2020

Yumin Zhang,[1,2] Chunqi Wang,[1,2] and Lixi Huang[1,2,a)]

AFFILIATIONS

[1]Department of Mechanical Engineering, The University of Hong Kong, Pokfulam, Hong Kong, China
[2]Lab for Aerodynamics and Acoustics, Zhejiang Institute of Research and Innovation, The University of Hong Kong, Hangzhou 311305, Zhejiang, China

[a)]Author to whom correspondence should be addressed: lixi.huang@hku.hk

ABSTRACT

An acoustic switch permits or forbids sound transmission through a partition, and its performance is governed by the stiffness and mass laws at low and high frequencies, respectively. The mechanism of artificial mass and stiffness, either positive or negative, is required to break these laws; all are demonstrated experimentally in this study. The switch consists of a suspended diaphragm with electric moving coil and a magnetic field, shunted by an essentially passive analog circuit. We show that electrically mediated damping is extremely large, and its mechanism as a powerful wave stopper can be very broadband, which contrasts with most resonance-based devices in the literature. We also show that a serial shunt capacitor introduces a mechanical mass that softens the diaphragm spring at low frequencies, while a shunt inductance is an electromagnetic spring that pacifies mechanical inertia at high frequencies. By manipulating the dynamic mass, stiffness, and damping electronically to enhance or defy the mass law and stiffness law, a switch effective in over one octave and working at a deep subwavelength scale is realized, and the maximum switch ratio is as high as 28 dB. As circuits can be miniaturized and easily tuned, these illustrated physics point to a versatile tool for digital control of sound waves.

An electric binary switch based on semiconductors is a fundamental unit of modern electronics. In this study, we aspire to build its acoustic counterpart: acoustic switch. An acoustic switch either blocks or permits the propagation of acoustic waves along a certain path. Potential applications include sound wave rectifiers, frequency modulators, noise isolators, and sound transmission enhancement.

Acoustic switches of various kinds were proposed in the past.[1–6] The current device distinguishes itself from these inventions without mechanically modifying the device. It also contrasts with other switches[7,8] or nonreciprocal (diode) devices[9–11] by operating purely in the linear regime. As shown in Fig. 1(a), the device is based on a moving-coil shunted by a passive circuit, and the switch effect is obtained by activating different circuits to achieve acoustically opaque or transparent states. As the coil moves in response to an incident sound, it cuts through the magnetic fields and the resulting mechanical force couples with the acoustic state. As will be explained in detail later, the acoustically opaque state, or the "switch-off" state, is achieved when the electromagnetic effect brings a very strong mechanical resistance, while the acoustic transparency, or the "switch-on" state, is realized when what we call an "electromagnetic spring" effect counters the mechanical mass in the system. This effect is similar to that of a mechanical spring used in a mass-in-mass[12] design of acoustic meta-material[13–15] where Newton's law appears violated if we choose to disregard the energy stored in the spring. Similar storage occurs in our electromagnetic spring used in the acoustic switch.

In general, near-complete sound reflection or absorption can be seen as a subset of acoustic switch functionality, namely, its switch-off state due to anti-resonance[14,15] (or dipolar vibration mode). In our configuration, the wave isolation is achieved through the high system resistance offered by the shunt circuit, while the mechanical part still operates in the monopole mode, contrasting with the classic dipole mode used for suppressing noise radiation.[16] The passive shunt circuit design in the current device also differs from the active control implementation in various metamaterial cells.[17–22] It is argued that it is easier to miniaturize a passive unit cell to form periodical arrays as metamaterial with tunable, appropriately homogenized density and bulk modulus[23,24] with potential applications like full-wave rectification contrasting the existing energy flow retification,[7,8] sound transmission, isolation,[14] or absorption reinforcement,[25] cloaking,[26] or super-lensing,[27] as well as other sound wave manipulations.

To introduce the so-called mass law and stiffness law, the transmission loss (TL) for a normal-incident sound through a suspended partition[28] is given as follows:

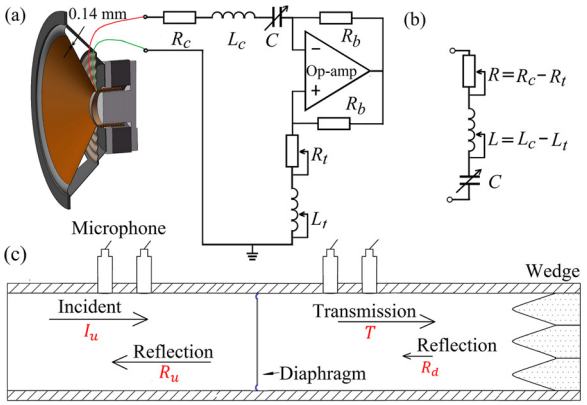

FIG. 1. The acoustic switch. (a) Loudspeaker shunted by an operational amplifier (op-amp) circuit. The mass of the moving diaphragm is $m_0 = 8.3$ g, and the stiffness is $k_0 = 17.0$ kN/m, giving a resonance frequency of 222 Hz. The magnetic strength of the loudspeaker is $Bl = 6.9$ T m. (b) R–L–C circuit equivalent to the circuit network in (a). Two sets of shunt circuit parameters (shunt-1 and shunt-2) are used in the tests. Shunt-1: $R_1 = 0.25\,\Omega$, $L_1 = 213\,\mu$H, and $C_1 = 248\,\mu$F; shunt-2: $C_2 = \infty$ (no capacitor), $R_2 = 0.34\,\Omega$, and $L_2 = 591\,\mu$F. The quoted resistance and inductance values already include the contributions from the coil. (c) Schematic of the test sample in the impedance tube, with a cross section of $A = 0.1$ m $\times$ 0.1 m.

$$\mathrm{TL} \equiv 10\log_{10}|I/T|^2,\ |I/T| = \frac{\sqrt{(\omega m - k/\omega)^2 + (\delta + 2Z_0)^2}}{2Z_0}, \quad (1)$$

where I and T are the pressure amplitudes of the incident and transmitted waves, respectively, m, k, and δ are the net acoustic mass, stiffness, and damping of the partition, respectively, $Z_0 = \rho_0 c_0 A$ is the acoustic impedance of air of the wave guide, ρ_0 and c_0 are the air density and sound speed, respectively, and ω is the angular frequency. The mechanical system has a resonance frequency of $\omega_0 = \sqrt{k/m}$. Equation (1) is simplified as $|I/T| = m\omega/(2Z_0)$ for $\omega \gg \omega_0$ and $|I/T| = k/(2Z_0\omega)$ for $\omega \ll \omega_0$. The mass law and stiffness law dominate high and low frequencies, respectively. The full model of Eq. (1) is called the suspended model and is often more appropriate to assess the performance of many composite structures or meta-atom designs. This work reports an approach to modify the system mass, stiffness, and damping properties in the broadband.

A common moving-coil loudspeaker shunted by an R–L–C circuit as shown in Fig. 1(a) is installed in an impedance tube as shown in Fig. 1(c). Microphone pairs are used to measure and decompose the standing waves,[29] I_u and R_u, for the determination of transmission loss, $\mathrm{TL} = 20\log_{10}|I_u/T|$, as well as the normalized acoustic impedance of the device, $Z/Z_0 = (I_u - R_u)/(I_u + R_u) - Z_d/Z_0$, where Z_d accounts for the downstream impedance, from which the damping $\delta = \mathrm{Re}(Z)$ and reactance $\chi = \mathrm{Im}(Z)$ are extracted.

The op-amp with two identical resistors R_b, forming a negative-impedance-converter,[30] serves for no other purposes but reducing the electrical resistance of the moving coil. Positive net resistance is kept constant, and no additional energy is input to the loudspeaker. The device is essentially passive. Op-amp can be removed if a coil with sufficiently low resistance is used.

When a sound wave with sound pressure p forces the diaphragm vibrating with velocity v, the coil moves along with it and cuts the magnetic field. An electromotive force of Blv is generated, which drives the current of $i_e = Blv/Z_e$ flowing across the circuit. Here, Z_e is the total electric impedance in the circuit. The Lorentz force applied on the charged moving coil is $F_e = Bli_e$, which couples with the acoustic velocity response (v) of the diaphragm and gives the electromagnetically induced (EMI) acoustic impedance as

$$\Delta Z \equiv F_e/v = (Bl)^2/Z_e, \quad Z_e = R + i(\omega L - 1/\omega C), \quad (2)$$

where L and C are the inductance and capacitance of the circuit, respectively. The impedance may be decomposed into resistive ($\Delta\delta$) and reactive ($\Delta\chi$) components as follows:

$$\Delta Z = \Delta\delta + i\Delta\chi, \quad \Delta\chi \approx \Delta m\omega - \Delta k/\omega. \quad (3)$$

Here, Δm and Δk are the EMI mass and stiffness, respectively. The total system resistance, mass, and stiffness are the sums of the intrinsic diaphragm properties δ_0, m_0, *and* k_0 and the EMI components $\Delta\delta$, Δm, *and* Δk.

The typical EMI impedance obtained by parameters of shunt-1 listed in Fig. 1 is illustrated in Fig. 2(a), with subfigures 2(a1)–2(a3) showing the zoom-in views of reactance.

At the circuit resonance frequency of $\omega_e = \sqrt{1/LC}$, one has $Z_e = R$ and the EMI damping has its peak with $\Delta\delta = (Bl)^2/R$. The EMI reactance (thick solid line) has a twist around the resonance. The maximum and minimum values occur at

$$\omega_L = \left(-R + \sqrt{R^2 + 4L/C}\right)/2L \quad \text{and}$$
$$\omega_H = \left(R + \sqrt{R^2 + 4L/C}\right)/2L, \quad (4)$$

respectively, and these are marked in the zoom-in view around the resonance in Fig. 2(a2). The exact reactance curve is complex, but asymptotic analysis can be made for the three extreme frequencies of low, high, and around resonance,

$$\Delta m_C = C(Bl)^2, \quad \omega < \omega_L, \quad (5a)$$

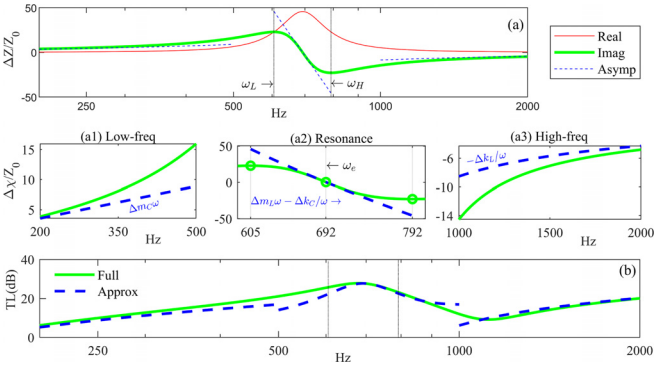

FIG. 2. Electromagnetically induced (EMI) acoustic impedance and predicted TL for the sample parameters given in the caption of Fig. 1. (a) Real and imaginary parts with asymptotic lines and zoom-in views from low to high frequencies (a1)–(a3). (b) Predicted TL in full (solid line) and with EMI approximations (dashed line). The approximate TL for the mid-frequency range is with EMI resistance only.

$$\Delta m_L = -(Bl)^2 L/R^2, \quad \Delta k_C = -(Bl)^2/(CR^2), \quad \omega_L < \omega < \omega_H, \tag{5b}$$

$$\Delta k_L = (Bl)^2/L, \quad \omega > \omega_H, \tag{5c}$$

where subscripts "C" and "L" indicate capacitor-dominated and inductor-dominated, respectively. The EMI mass and stiffness show very different characteristics as they have different physical origins. In the low-frequency range of $\omega < \omega_L$, the EMI reactance is dominated by a positive mass induced by the capacitor, denoted as Δm_C, while in the high frequency range of $\omega > \omega_H$, the EMI reactance is a positive spring derived from inductance and denoted by Δk_L. In the intermediate frequency range around the electric resonance, (ω_L, ω_H), the EMI reactance is a combination of negative dynamic mass ($\Delta m_L < 0$) and negative stiffness ($\Delta k_C < 0$) controlled by the inductance and capacitance, respectively. The zoom-in views shown in Figs. 2(a1)–2(a3) show that they are indeed appropriate at very low, around resonance, and very high frequencies.

For the high-frequency region $\omega > \omega_H$ in Fig. 2(a3), the Lorentz force is determined by the inductance $Ldi_e/dt = Blv$, and so the current i_e has a phase angle of $\pi/2$ behind the voltage or velocity v. This means that the current is in phase with the diaphragm displacement, say x, and hence, $Li_e = Blx$. The resulting Lorentz force against the motion, $F_e = Bli_e = x(Bl)^2/L$, is also proportional to the displacement x and is a positive spring with a constant of $\Delta k_L = (Bl)^2/L$. In the low frequency region $\omega < \omega_L$ shown in Fig. 2(a1), the circuit is dominated by the capacitance. The electric charge is related to the motion induced voltage Blv through $q = CBlv$. The current $i_e = dq/dt$ is then proportional to acceleration dv/dt, and hence, the reaction force $F_e = Bli_e = C(Bl)^2 dv/dt$ yields a pure inertia equal to $\Delta m_C = C(Bl)^2$.

Near electrical resonance frequency ω_e, resistance dominates the Lorentz force and the electromagnetic force, $F_e = Bli_e = v(Bl)^2/R$, is in phase with the velocity and presents a mechanical resistance $\Delta\delta = (Bl)^2/R$, which is inversely proportional to the electrical resistance R. When R is small, it presents a huge mechanical damping (energy transfer to the electrical sink) that can block sound from transmission (see below).

When the EMI reactance is approximated by the constant EMI mass, resistance, and stiffness given in Eqs. (5), the TL is approximated in various frequency regions and is shown in dashed lines in Fig. 2(b). The full TL (solid curve) and approximations (dashed lines) agree well. Note that, around the electric resonance ω_e, the approximation for the EMI impedance is to keep the resistance only as the reactance is low. The fact that the full TL is broader than this approximation implies that the double negativity helps in a marginal manner.

The proposition that the EMI mass and spring may be used to both increase and decrease sound transmission needs to be tested. Equation (1) shows that, to increase TL, one either increases system damping or increases reactance, or both. The opposite is required to decrease TL. Parameters of the two shunt circuits used are listed in the caption of Fig. 1, together with the intrinsic mechanical properties of the sample loudspeaker.

Figure 3(a) shows the TL for the base unit (shunt-off, thin-black-solid curve) and that with shunt-1 (thick-red-solid curve). The latter is compared with the prediction (dashed curve) based on the base unit impedance measured plus the theory for the EMI impedance given in Eq. (2). The agreement is satisfactory. The two TL curves crossover at two frequencies, 176 Hz and 927 Hz, forming three regions marked by different colors.

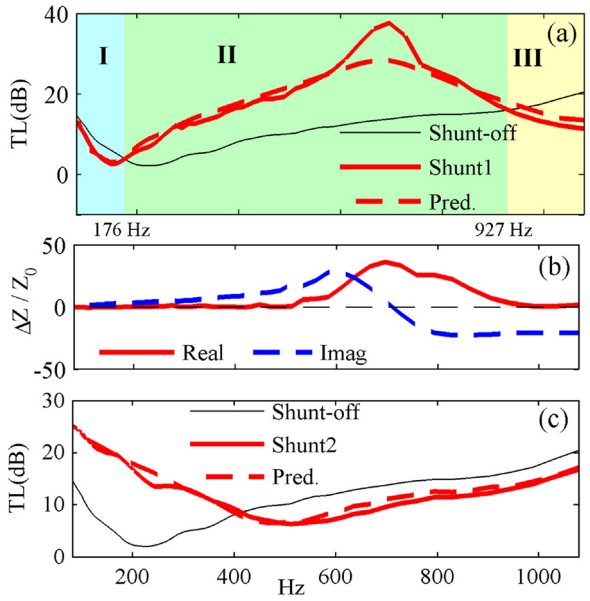

FIG. 3. Experimental results of the device without and with two shunt circuits. (a) TL at shunt-off (thin-solid curve) and shunt-1 (thick curves, solid for experiment, and dashed for prediction) with frequency regions marked for acoustic transparency (I and III) and opaqueness (II) effects by shunt-1. (b) The EMI reactance (dashed) and damping (solid line) for shunt-1. (c) Comparison of TL for shunt-2 between experiment (solid) and prediction (dashed).

Region I lies left to the intrinsic resonance frequency of 222 Hz and is, therefore, stiffness controlled. The positive EMI mass derived from the capacitor [cf. Fig. 2(a1), Eq. 5(a)] overcomes part of the system stiffness and brings acoustic transparency. The maximum improvement is 3.4 dB at 143 Hz. In region III, which is mass-law controlled, the EMI spring [cf. Eq. 5(c), Fig. 2(a3)] counters the system mass. Here, we see much more acoustic transparency brought by the shunt circuit than region I. In region II, the shunt circuit delivers acoustic opaqueness or vibration isolation. The main physical ingredient at play is the EMI damping, accompanied by the reactance reduction due to the negative EMI mass and stiffness. At 695 Hz, the TL for the shunt-on is 24 dB higher than that for the shunt-off. This means that the transmitted sound energy is only 0.4% of that when the shunt circuit is off.

Figure 3(b) shows the measured EMI damping (solid line) and reactance (dashed line), which agrees with the trend shown in Fig. 2(a), where different scales and frequency ranges are used. Figure 3(c) compares the TL for shunt-2 between experimental data (solid line) and the prediction (dashed line), also with good agreement. Note that shunt-2 has no capacitor, and two EMI effects are expected: positive damping and positive spring. Damping raised the TL in the low frequency region below about 400 Hz, while the EMI spring overcomes the system mass and decreases TL above 400 Hz. The TL trough is moved from 222 Hz for shunt-off to 511 Hz for shunt-2.

Both shunt circuits deliver increased and decreased TL in different frequency regions. We now put them together to form a two-way switch. The results are shown in Fig. 4.

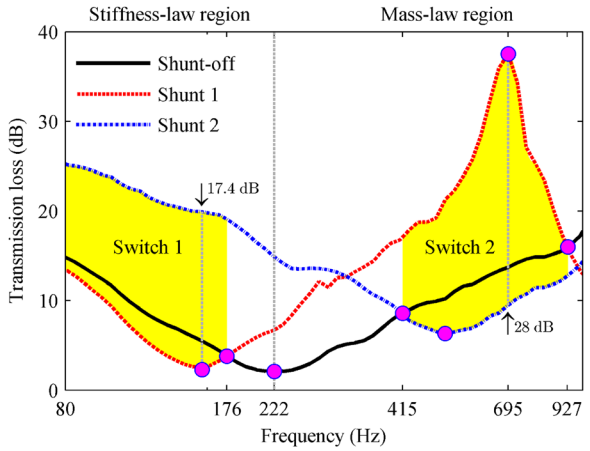

FIG. 4. Effective frequency ranges (colored areas) of the acoustic switch formed by three transmission loss curves, in which the shunt-off TL performance is sandwiched between the two shunted performance curves. Switch 1 operates in the stiffness-controlled region and switch 2 in the mass-law region. Maximum switch ratios and other importance frequencies and TL numbers are marked.

Two valid switch regions are found and colored in the figure. The low-frequency region of "switch 1" runs from 80 Hz to 176 Hz, defying the stiffness law, and the switch ratio is high up to 17.4 dB as marked in the figure. "Switch 2" is from 413 to 927 Hz, violating the mass law, and its switch ratio is high up to 28 dB. Both switches are over one octave effective band. It is possible that design optimization may further extend the frequency scope of these switches as well as the switching ratio defined as the difference between the switch-off and switch-on values of TL.

EMI damping may be called an electromagnetic dashpot. It transfers mechanical energy into electrical energy. Its effect is inversely proportional to electrical resistance. Theoretically, infinite damping ensures when the shunt bypass is short-circuited; the effect is broadband as damping is essentially frequency independent. Figure 4 clearly shows that more sound is blocked over 2.4 octave, from 176 to 927 Hz for shunt-1 and from the DC frequency to 413 Hz for shunt-2, which is over four octave bands counting from 20 Hz. The shunted lead zirconate titanate (PZT) plate can also achieve the tunable switching effect.[31,32] However, it is unlikely that a PZT device will deliver a performance higher than two octaves of the acoustic switch in air due to the low electromechanical coupling efficiency and the inherent high bending stiffness.

Near the electric resonance, the negative EMI mass and stiffness are found, but their effect on sound transmission is dominated by the strong dashpot effect. Away from the electric resonance, both the EMI mass and stiffness are positive. The positive EMI mass counters the mechanical spring at low frequency, and it improves the acoustic transparency. Likewise, EMI stiffness, which is an electromagnetic spring, overcomes inertia in the high-frequency, mass-law region. It is emphasized here that the breaking of both the mass law and the stiffness law here is much higher than that by the double negativity. The latter is closely related to the phase change around resonance.

In summary, two attributes are highlighted. One is the passive nature of the device, and the other is the potential to intelligently manipulate the mechanical properties and hence sound propagation with the full power of electronics. Such an acoustic switch may function as a fundamental unit for sound propagation manipulation, and frequency modulators, artificial dipoles, perfect matching layers, and so on may be derived from the current switch.

AUTHORS' CONTRIBUTIONS

All the authors contributed equally to this work.

This work was supported by the National Science Foundation of China, Project No. 51775467, and a block grant from the Hangzhou Municipal Government.

The data that support the findings of this study are available within this article.

REFERENCES

[1]P. Wang, F. Casadei, S. Shan, J. C. Weaver, and K. Bertoldi, Phys. Rev. Lett. **113**, 014301 (2014).
[2]M. Schirber, Physics **7**, s79 (2014).
[3]F. Wu, Z. Liu, and Y. Liu, Phys. Rev. E **66**, 046628 (2002).
[4]S. Babaee, N. Viard, P. Wang, N. X. Fang, and K. Bertoldi, Adv. Mater. **28**, 1631 (2016).
[5]G. Ma, X. Fan, P. Sheng, and M. Fink, Proc. Natl. Acad. Sci. **115**, 6638 (2018).
[6]C. Vanhille and C. Campos-Pozuelo, Ultrason. Sonochem. **21**, 50 (2014).
[7]N. Boechler, G. Theocharis, and C. Daraio, Nat. Mater. **10**, 665 (2011).
[8]F. Li, P. Anzel, J. Yang, P. G. Kevrekidis, and C. Daraio, Nat. Commun. **5**, 5311 (2014).
[9]X. F. Li, X. Ni, L. Feng, M. H. Lu, C. He, and Y. F. Chen, Phys. Rev. Lett. **106**, 084301 (2011).
[10]B. Liang, X. S. Guo, J. Tu, D. Zhang, and J. C. Cheng, Nat. Mater. **9**, 989 (2010).
[11]B. Liang, B. Yuan, and J. C. Cheng, Phys. Rev. Lett. **103**, 104301 (2009).
[12]G. W. Milton and J. R. Willis, Proc. R. Soc. A **463**, 855 (2007).
[13]J. B. Pendry and J. Li, New J. Phys. **10**, 115032 (2008).
[14]Z. Yang, J. Mei, M. Yang, N. H. Chan, and P. Sheng, Phys. Rev. Lett. **101**, 204301 (2008).
[15]Z. Liu, X. Zhang, Y. Mao, Y. Y. Zhu, Z. Yang, C. T. Chan, and P. Sheng, Science **289**, 1734 (2000).
[16]G. Koopman, *Designing Quiet Structures: A Sound Power Minimization Approach* (Academic Press, San Diego, 1997).
[17]B. I. Popa, L. Zigoneanu, and S. A. Cummer, Phys. Rev. B **88**, 024303 (2013).
[18]R. Fleury, D. Sounas, and A. Alù, Nat. Commun. **6**, 5905 (2015).
[19]C. Shi, M. Dubois, Y. Chen, L. Cheng, H. Ramezani, Y. Wang, and X. Zhang, Nat. Commun. **7**, 11110 (2016).
[20]B. I. Popa and S. A. Cummer, Nat. Commun. **5**, 3398 (2014).
[21]B. I. Popa, Y. Zhai, and H. S. Kwon, "Broadband sound barriers with bianisotropic metasurfaces," Nat. Commun. **9**(1), 5299 (2018).
[22]Y. Zhai, H. S. Kwon, and B. I. Popa, "Active Willis metamaterials for ultracompact nonreciprocal linear acoustic devices," Phys. Rev. B **99**(22), 220301 (2019).
[23]J. Li and C. T. Chan, Phys. Rev. E **70**, 055602(R) (2004).
[24]J. G. Berryman, J. Acoust. Soc. Am. **68**, 1809 (1980); **68**, 1820 (1980).
[25]J. Mei, G. Ma, M. Yang, Z. Yang, W. Wen, and P. Sheng, Nat. Commun. **3**, 756 (2012).
[26]S. A. Cummer, J. Christensen, and A. Alù, Nat. Rev. Mater. **1**, 16001 (2016).
[27]L. Fok, M. Ambati, and X. Zhang, MRS Bull. **33**, 931 (2008).
[28]F. J. Fahy and P. Gardonio, *Sound and Structural Vibration: Radiation, Transmission and Response* (Elsevier, Burlington, 2007), Chap. 5.
[29]J. Y. Chung and D. A. Blaser, J. Acoust. Soc. Am. **68**, 907 (1980); **68**, 914 (1980).
[30]W. K. Chen, *The Circuits and Filters Handbook* (CRC Press, Boca Raton, 2009), Chap. 13.
[31]J. A. B. Gripp, L. C. Goes, O. Heuss, and F. Scinocca, Smart Mater. Struct. **24**, 125017 (2015).
[32]A. Baz, J. Acoust. Soc. Am. **143**, 1376 (2018).